

# First- and second-harmonic detection of spin accumulation in a multiterminal lateral spin valve under high-bias ac current

Shaojie Hu,<sup>1</sup> Tatsuya Nomura,<sup>2</sup> Ginga Uematsu,<sup>2</sup> Nagarjuna Asam,<sup>2</sup> and Takashi Kimura<sup>1,2,\*</sup>

<sup>1</sup>*Research Center for Quantum Nano-Spin Sciences, Kyushu University, 744 Motoooka, Fukuoka 819-0395, Japan*

<sup>2</sup>*Department of Physics, Kyushu University, 744 Motoooka, Fukuoka 819-0395, Japan*

(Received 30 March 2016; revised manuscript received 9 June 2016; published 13 July 2016)

We have investigated the transport properties of electrically and thermally excited spin currents in a lateral spin valve consisting of a spin injector and detector with a middle ferromagnetic wire by detecting the first- and second-harmonic voltages. The first-harmonic spin signal was significantly suppressed by the middle ferromagnetic wire because of the spin absorption effect. On the other hand, in the second-harmonic signal, a small signal related to the middle ferromagnetic wire was observed in addition to a conventional spin signal with a reduced magnitude. This indicates that the additional ferromagnetic wire acts not only as the spin absorber but also as another spin injector under thermal spin injection, because the heat current caused by direct spin injection propagates to the middle ferromagnetic wire and creates another temperature gradient. By using this effect, we show that the magnetization direction of a ferromagnetic nanodot embedded in a nonmagnetic Cu wire becomes measurable.

DOI: [10.1103/PhysRevB.94.014416](https://doi.org/10.1103/PhysRevB.94.014416)

## I. INTRODUCTION

The electronic device utilizing electron spins is one of the promising approaches for next-generation nanoelectronic devices [1,2]. Especially, the establishment of a concept of spin current, the flow of the spin angular momentum, provides two important progresses in the operation of spin-based electric devices [3]. One is the manipulation of the electric current originating from spin-dependent transports such as giant magnetoresistance [4,5] and tunnel magnetoresistance [6–8]. The electric signal reflecting the spin information enables us to detect the magnetization direction precisely and sensitively [9,10]. The other one is the manipulation of the magnetization direction due to the transfer of the spin angular momentum [11–13]. The injection of spin current into a small ferromagnet exerts the torque on the local magnetization and provides a reliable magnetization switching technique with low power consumption [14,15]. Thus, these innovative techniques based on electrical means offer a highly selectable architecture, which seems to be suitable for an integrated circuit. However, the preparation of nanoscale magnetic multilayers with individual electrodes significantly complicates the fabrication procedure of nanoelectronic devices. Therefore, seamless device integration is an important milestone for developing nanospin devices as well as energy efficient device operation.

Apart from the electrical control of the spin current, recently, the manipulation of spin currents using heat has been paid considerable attention under the concept of spin caloritronics combining spintronics and thermoelectrics [16–20]. Numerous intriguing phenomena such as spin Seebeck [16], spin-dependent Seebeck [17], spin-dependent Peltier, and spin Peltier effects [21,22] have been reported in various structures. Moreover, the spin transfer torque induced by thermally excited spin currents was also studied theoretically [23,24] and experimentally [25–28]. Although some of the devices consisting of simple ferromagnetic/nonmagnetic

hybrid structures are suitable for mass production [29], the study on thermally excited spin currents reported so far mainly focuses on fundamental viewpoints. The performance at the moment is quite far from a practical application because of the low efficiencies of the related effects. We have demonstrated that CoFeAl shows an excellent performance for thermal spin injection because of its large spin-dependent Seebeck coefficient [30]. This may open up possibilities for utilizing the heat-induced spin current in a practical device. Moreover, a high thermal spin-injection efficiency provides the ideal platform for a detailed experimental study on the thermally excited spin current. Especially, the transport properties of the thermally excited spin current in multiterminal lateral hybrid structures have not been well studied. Here, we investigate the spin absorption property due to an additional ferromagnetic wire under thermal spin injection. We found that the thermally excited spin signal was strongly modulated by an additionally connected middle ferromagnetic wire. By extending this property, we propose and demonstrate that the magnetization direction of the middle wire can be indirectly detected by using thermal spin injection. The waste heat due to the electric current, namely, Joule heating, enables one to induce additional spin injection, leading us to distinguish the magnetization direction without an independent electrode.

## II. EXPERIMENTAL PROCEDURE

Figure 1 shows a scanning electron microscope image of a lateral spin valve device used for the present study, together with a schematic illustration. We fabricated the lateral spin valve consisting of three ferromagnetic CoFeAl (CFA) wires bridged by a Cu strip. The device was fabricated by two-step lift-off processes. First, three CFA wires, 40 nm in thickness and 120 nm in width, were deposited by electron-beam evaporation on a thermally oxidized Si substrate under a base pressure of  $2.0 \times 10^{-7}$  Pa. Here, the center-to-center distances for two neighboring CFA wires are 300 nm. In order to control the relative configuration of the magnetizations for three CFA wires by adjusting the magnetic field, the differences in the

\*t-kimu@phys.kyushu-u.ac.jp

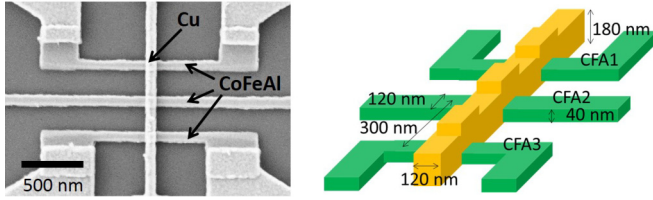


FIG. 1. Scanning electron microscope (SEM) image of the fabricated lateral spin valve consisting of three CoFeAl wires bridged by a Cu strip, together with a schematic illustration of the device geometry.

edge shapes for the CFA wires were introduced. Then, a Cu strip (120 nm wide and 150 nm thick) bridging the CFA wires was thermally evaporated. The electrical resistivities for Cu and CFA are, respectively, 2.2 and 45.0  $\mu\Omega$  cm. Prior to Cu deposition, the CFA surfaces were carefully cleaned by low power Ar ion milling to obtain a highly transparent interface with a few m $\Omega$  interface resistance. The electrically and thermally excited spin transports were detected using a low-frequency lock-in technique with first- and second-harmonic voltage responses, respectively. Here, all the measurements were performed in air at room temperature.

### III. RESULTS AND DISCUSSIONS

First, we evaluated the electrical spin-injection and detection property of the fabricated lateral spin valve device from a conventional nonlocal spin valve measurement. Figure 2(a) shows a room-temperature spin signal using the CFA1 injector and CFA2 detector. A clear large spin valve signal with a magnitude of 4.2 m $\Omega$  assures a high electrical spin polarization

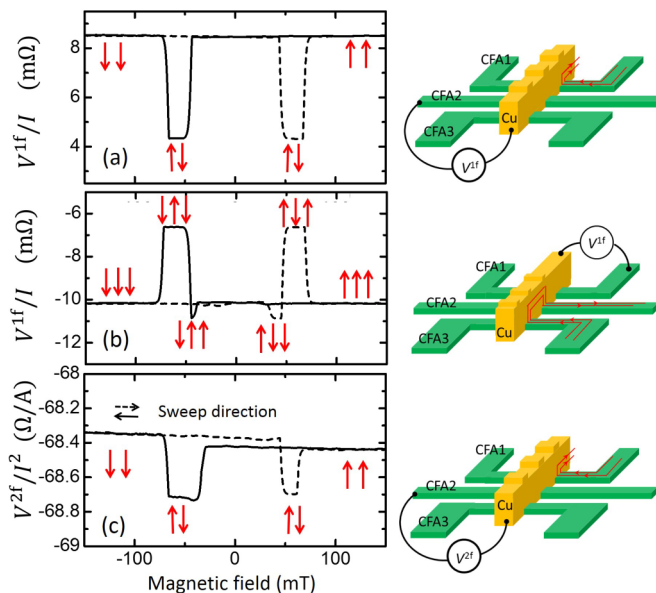


FIG. 2. (a) Room-temperature first-harmonic spin valve signal using a CFA1 injector and CFA2 detector. (b) First-harmonic spin valve signal detected by CFA1 under spin injection from CFA2 to CFA3. (c) Second-harmonic spin valve signal detected by CFA2 under thermal spin injection using CFA1. The right-hand sides for each figure correspond to the probe configuration for the measurements.

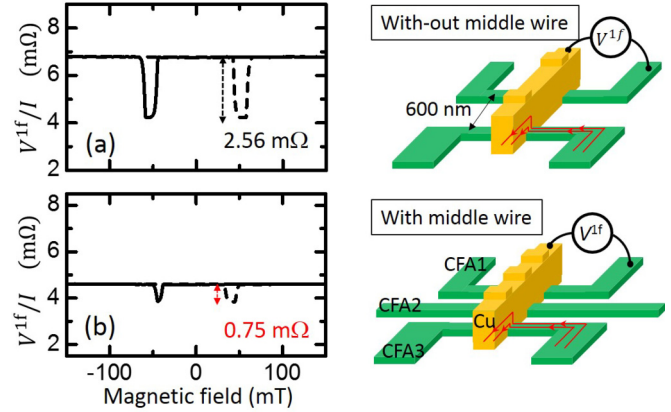


FIG. 3. Room-temperature first-harmonic spin valve signal for a standard CFA/Cu lateral spin valve (a) without the middle CFA wire and (b) with the middle CFA wire. In both devices, the center-to-center distance between the injector and the detector is 600 nm.

for the CFA wires with ideal interface conditions. We also confirmed that the interface for the CFA3/Cu is also in an ideal condition from nonlocal detection with multiterminal spin injection, where the spin signal detected by CFA1 is modified by the relative magnetization configuration of CFA2 and CFA3 [35]. As shown in Fig. 2(b), a spin signal with a magnitude comparable to Fig. 2(a) and its modulation depending on the relative magnetization configuration between CFA2 and CFA3 were clearly confirmed. We also evaluated the thermal spin-injection property from the second-harmonic voltage measurements. As shown in Fig. 2(c), a clear spin valve signal has been observed at room temperature, assuring that the spin-dependent Seebeck coefficient for our CFA wire was sufficiently large, but the value is slightly smaller than our previous reports [30]. This is because the relatively thicker Cu and CFA wires reduce the temperature gradient at the same current. A small asymmetry with respect to the magnetic field is due to the anomalous Nernst-Ettingshausen effect induced in the CFA2 detector [19].

We then evaluated the spin absorption property for the CFA wire. We fabricated a conventional CFA/Cu lateral spin valve with a center-to-center distance of 600 nm and performed a nonlocal spin valve measurement for comparison. As shown in Fig. 3(a), we obtained a clear bipolar spin signal with the magnitude of 2.56 m $\Omega$ , which is a reasonable value compared to previous reports. We then measured the room-temperature spin signal with the middle absorber by using the device shown in Fig. 1. Because of the high electrical spin polarization for CFA, we still clearly observed bipolar spin signals with a magnitude of 0.75 m $\Omega$  even in the device with the middle CFA absorber, as indicated in Fig. 3(b). Here, we quantitatively evaluate the absorption efficiency. From the spin transport model with a transparent interface, the ratio of the spin signal  $\eta$  can be analytically calculated as follows [31–34],

$$\eta = \frac{2[(1+Q)\cosh a + \sinh a]}{(2+3Q)\cosh a + (2+Q+Q^2)\sinh a}, \quad (1)$$

where  $Q$  is defined as  $R_{\text{Cu}}^S/R_{\text{CFA}}^S$ , which is the ratio of the spin resistance for Cu  $R_{\text{Cu}}^S$  to that for CFA  $R_{\text{CFA}}^S$ .  $a$  is defined as  $l/2\lambda_{\text{Cu}}$  with a center-to-center distance between the

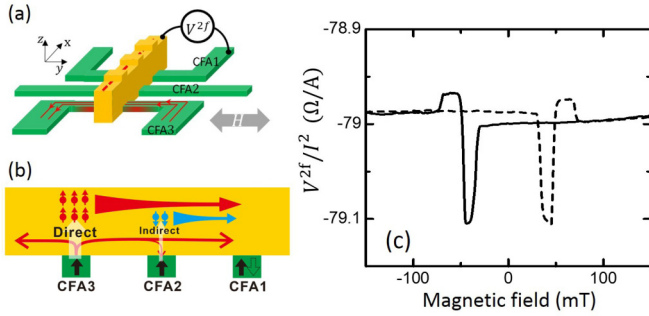


FIG. 4. (a) Schematic illustration of the thermal spin injection and detection in a lateral spin valve with the middle CFA wire, together with the probe configuration for the measurement. (b) Heat flow under thermal spin injection in the triple CFA/Cu junction and induced spin accumulation in the Cu strip. (c) Room-temperature second-harmonic spin valve signal observed in the CFA/Cu lateral spin valve with the middle CFA wire.

injector and detector  $l$  and the spin diffusion length for Cu. By using the values obtained from the separately performed experiments ( $\lambda_{\text{Cu}} = 500$  nm and  $P_{\text{CFA}} = 0.65$ ),  $R_{\text{Cu}}^{\text{S}}$  and  $R_{\text{CFA}}^{\text{S}}$  can be calculated as 1.22 and 0.20  $\Omega$ , respectively, leading to  $Q = 6.0$ . As a result, we obtain  $\eta$  as 0.35, which is in reasonable agreement with the experimentally obtained value (0.29). This indicates that the interface condition between CFA/Cu is highly transparent.

We evaluate the absorption property of the thermally excited spin current by using the second-harmonic voltage detection with the probe configuration shown in Fig. 4(a). Interestingly, a small negative voltage change has been observed in addition to the main spin valve signal changes due to injector and detector switching. By comparing the field dependence of the signal shown in Fig. 2(b), we conclude that the additional resistance change around 70 mT was caused by the magnetization switching of CFA2. According to the nonlocal detection scheme, the detecting voltage depends on the relative angle between the spin injector and detector. Therefore, it is not so simple to explain the reason for the appearance of the additional signal change due to the magnetization switching of CFA2. To understand the reason for the additional signal, we consider the heat flow in the present sample. Since the Cu has a high thermal conductivity, the heat generated in the CFA3 easily propagates into the CFA2. This produces a temperature gradient across the Cu/CFA2 junction, resulting in thermal spin injection from CFA2 into the Cu. Therefore, as schematically shown in Fig. 4(b), in the heat-related second-harmonic signal for detecting the heat-related signal, the thermal spin injections both from CFA3 and CFA2 should be considered. Here, it should be noted that the direction of the temperature gradient in the CFA2/Cu junction is in the opposite direction to that in the CFA3/Cu junction. Therefore, the sign of spin signal due to CFA2 switching should be reversed to that of CFA3. As shown in Fig. 4(c), the spin signal due to CFA2 switching was negative, which was indeed opposite to that of CFA3 [17,30]. Moreover, we confirmed that the additional voltage change shows parabolic dependences on the magnitude of the ac current as well as the main two voltage changes. Thus, the additional spin signal observed in Fig. 4(b) can be understood

by thermal spin injection from CFA2. Moreover, this result indicates that one can distinguish the magnetization direction without using direct spin injection and detection.

We quantitatively evaluate the magnitude of the thermal spin signal induced by indirect spin injection from CFA2. According to the one-dimensional spin diffusion model, the thermally induced spin voltage  $\Delta V_{\text{S}}$  under the temperature gradient  $\nabla T$  of the CFA in the vicinity of the CFA/Cu interface, in a conventional CFA/Cu lateral spin valve with a separation distance  $l$ , is given by the following equation,

$$\Delta V_{\text{S}} = \frac{Q P_{\text{CFA}} \lambda_{\text{CFA}} S_{\text{CFA}}^{\text{S}} \nabla T}{2(1+Q)(\cosh x + \sinh x) + Q^2 \sinh x}, \quad (2)$$

where  $x$  is the normalized separation distance defined by  $l/\lambda_{\text{Cu}}$ .  $P_{\text{CFA}}^{\text{S}}$  and  $S_{\text{CFA}}^{\text{S}}$  are the electrical spin polarization and the spin-dependent Seebeck coefficient for CFA, respectively. Since the diffusion process of the spin current does not depend on the excitation method, the spin voltage with the middle CFA  $\Delta V_{\text{S}}^{\text{Abs}}$  under thermal spin injection can be calculated as  $\eta \Delta V$  with a similar consideration of the absorption efficiency  $\eta$  discussed in the electrical scheme. Moreover, the spin voltage indirectly induced by the CFA2  $\Delta V_{\text{S}}^{\text{Ind}}$  can be approximately calculated by assuming the temperature gradient of the CFA2 in the vicinity of the CFA2/Cu interface  $\nabla T'$  with a normalized distance  $x/2$ . Therefore, the ratio of the spin voltage due to the CFA3 to that of CFA2  $\xi$  can be approximately given by the following equation,

$$\begin{aligned} \xi &= \frac{\Delta V_{\text{S}}^{\text{Ind}}}{\Delta V_{\text{S}}^{\text{Abs}}} \\ &\approx \frac{\nabla T'}{\eta \nabla T} \frac{2(1+Q)(\cosh x + \sinh x) + Q^2 \sinh x}{2(1+Q)[\cosh(x/2) + \sinh(x/2)] + Q^2 \sinh(x/2)}. \end{aligned} \quad (3)$$

Since  $\xi$  can be estimated experimentally to be 0.13 from the results shown in Fig. 4(a), we obtain the relation  $\nabla T' = 0.06 \nabla T$ .

To confirm the reliability of the above relationship, we have numerically calculated the spatial distributions of the current and the temperature of the present CFA/Cu lateral

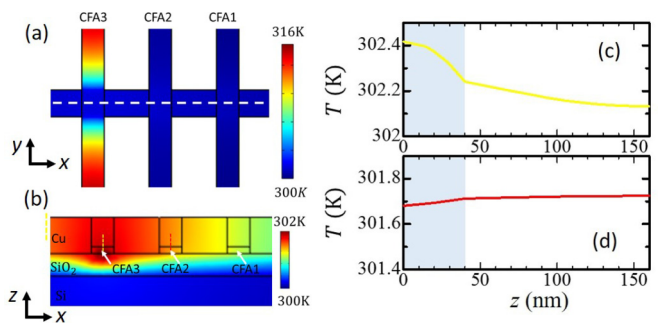


FIG. 5. Numerically simulated temperature distribution of the lateral spin valve under a bias current of 0.63 mA at ambient temperature. (a) Top view of the temperature profile in the  $x$ - $y$  plane. (b) Cross-sectional view of the temperature profile in the  $x$ - $z$  plane. Line profiles of the temperature distributions along the  $z$  axis (c) at the center of the CFA1/Cu junction and (d) that at the center of the CFA2/Cu junction.

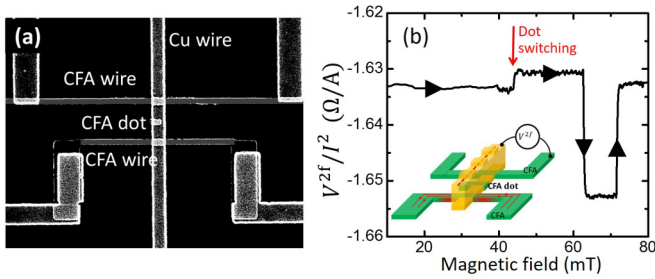


FIG. 6. (a) SEM image of the fabricated lateral spin valve with a ferromagnetic nanodot embedded in a Cu wire. (b) Second-harmonic voltage as a function of the magnetic field, which is swept from the negative to the positive direction. The inset shows a schematic illustration of the probe configuration for the measurement.

spin valve under a bias current  $I_{ac} = 0.63$  mA in CFA3 by using the finite element program COMSOL MULTIPHYSICS. Here, we assume that the thermal conductivities for Cu, CFA, Si, and  $\text{SiO}_2$  are 400, 29.8, 130, and  $1.4 \text{ W m}^{-1} \text{ K}^{-1}$ , respectively. Figures 5(a) and 5(b) show the three-dimensional color plots of the simulated temperature for the lateral and vertical profiles, respectively. CFA and Cu wires are aligned along  $x$  and  $y$ , respectively.  $z$  is the direction normal to the junction. From the results, we confirmed that the heat flow effectively propagated in the Cu wire and reached the CFA2. As can be seen in Figs. 5(c) and 5(d), the temperature gradient along the  $z$  direction at the CFA2/Cu junction is found to be approximately 5% of that at the CFA3/Cu junction, which shows good agreement with the experimental estimation. Thus, the additional signal observed in Fig. 4(c) is quantitatively explained by indirect spin injection from CFA2.

Finally, we demonstrate that the magnetization direction of a small ferromagnetic nanodot embedded in a Cu wire can be detected by using the present indirect detection method. Figure 6(a) shows the fabricated lateral spin valve for this

study. Here, the CFA nanodot was placed underneath the Cu wire between the CFA injector and CFA detector. It is impossible to detect the magnetization direction by using the conventional electrical detection scheme. However, as can be seen in Fig. 6(b), by using the second-harmonic detection technique, we have clearly obtained a positive sudden signal change, which is caused by a magnetization reversal of the CFA nanodot. Although the obtained signal change in the present measurement is not so large, the magnitude of the signal will be improved by the optimizations of the device geometry, such as reducing the distance between the injector and nanodot and enhancing the heat conductivity of the nanodot.

#### IV. CONCLUSION

In summary, we have investigated the electrically and thermally excited spin current transports in a CoFeAl/Cu lateral spin valve with a middle CoFeAl wire. In conventional nonlocal spin detection, the spin signal expectedly shows a significant reduction due to the spin current absorption effect. On the other hand, in the second-harmonic detection, an unexpected additional signal change depending on the magnetization direction of the middle wire has been observed in addition to the conventional thermal spin signal. We found that this additional signal is quantitatively explained by indirect thermal spin injection from the middle wire due to the heat flow through the Cu strip. By using this scheme, we have succeeded in detecting the magnetization direction of the ferromagnetic nanodot embedded in a nonmagnetic channel.

#### ACKNOWLEDGMENT

This work is partially supported by Grant-in-Aid for Scientific Research on Innovative Area, ‘‘Nano Spin Conversion Science’’ (26103002) and that for Scientific Research (S)(25220605) from Ministry of Education, Culture, Sports, Science and Technology in Japan.

- [1] S. A. Wolf, D. D. Awschalom, R. A. Buhrman, J. M. Daughton, S. von Molnar, M. L. Roukes, A. Y. Chtchelkanova, and D. M. Treger, *Science* **294**, 1488 (2001).
- [2] I. Žutić and S. Das Sarma, *Rev. Mod. Phys.* **76**, 323 (2004).
- [3] E. Saitoh, T. Kimura, S. Maekawa, and S. O. Valenzuela, *Spin Current* (Oxford University Press, Oxford, UK, 2012).
- [4] M. N. Baibich, J. M. Broto, A. Fert, F. Nguyen Van Dau, F. Petroff, P. Etienne, G. Creuzet, A. Friederich, and J. Chazelas, *Phys. Rev. Lett.* **61**, 2472 (1988).
- [5] G. Binasch, P. Grünberg, F. Saurenbach, and W. Zinn, *Phys. Rev. B* **39**, 4828 (1989).
- [6] J. S. Moodera, L. R. Kinder, T. M. Wong, and R. Meservey, *Phys. Rev. Lett.* **74**, 3273 (1995).
- [7] T. Miyazaki and N. Tezuka, *J. Magn. Magn. Mater.* **139**, L231 (1995).
- [8] S. S. P. Parkin, K. P. Roche, M. G. Samant, P. M. Rice, R. B. Beyers, R. E. Scheuerlein, E. J. O. Sullivan, S. L. Brown, J. Bucchigano, D. W. Abraham, Y. Lu, M. Rooks, P. L. Trouilloud, R. A. Wanner, and W. J. Gallagher, *J. Appl. Phys.* **85**, 5828 (1999).
- [9] T. Kimura, Y. C. Otani, and P. M. Levy, *Phys. Rev. Lett.* **99**, 166601 (2007).
- [10] S. Nonoguchi, T. Nomura, and T. Kimura, *Phys. Rev. B* **86**, 104417 (2012).
- [11] J. Slonczewski, *J. Magn. Magn. Mater.* **159**, L1 (1996).
- [12] E. B. Myers, D. C. Ralph, J. A. Katine, R. N. Louie, and R. A. Buhrman, *Science* **285**, 867 (1999).
- [13] J. A. Katine, F. J. Albert, R. A. Buhrman, E. B. Myers, and D. C. Ralph, *Phys. Rev. Lett.* **84**, 3149 (2000).
- [14] T. Kimura, Y. Otani, and J. Hamrle, *Phys. Rev. Lett.* **96**, 037201 (2006).
- [15] T. Yang, T. Kimura, and Y. Otani, *Nat. Phys.* **4**, 851 (2008).
- [16] K. Uchida, S. Takahashi, K. Harii, J. Ieda, W. Koshibae, K. Ando, S. Maekawa, and E. Saitoh, *Nature (London)* **455**, 778 (2008).
- [17] A. Slachter, F. L. Bakker, J.-P. Adam, and B. J. van Wees, *Nat. Phys.* **6**, 879 (2010).
- [18] G. E. W. Bauer, E. Saitoh, and B. J. van Wees, *Nat. Mater.* **11**, 391 (2012).
- [19] S. Hu and T. Kimura, *Phys. Rev. B* **87**, 014424 (2013).

- [20] C. Mu, S. Hu, J. Wang, and T. Kimura, *Appl. Phys. Lett.* **103**, 132408 (2013).
- [21] J. Flipse, F. L. Bakker, A. Slachter, F. K. Dejene, and B. J. van Wees, *Nat. Nanotechnol.* **7**, 166 (2012).
- [22] J. Flipse, F. K. Dejene, D. Wagenaar, G. E. W. Bauer, J. B. Youssef, and B. J. van Wees, *Phys. Rev. Lett.* **113**, 027601 (2014).
- [23] Z. Yuan, S. Wang, and K. Xia, *Solid State Commun.* **150**, 548 (2010).
- [24] X. Jia, K. Xia, and G. E. W. Bauer, *Phys. Rev. Lett.* **107**, 176603 (2011).
- [25] H. Yu, S. Granville, D. P. Yu, and J.-P. Ansermet, *Phys. Rev. Lett.* **104**, 146601 (2010).
- [26] L. Fitoussi, F. A. Vetro, C. Caspers, L. Gravier, H. Yu, and J. P. Ansermet, *Appl. Phys. Lett.* **106**, 162401 (2015).
- [27] G. Choi, B. Min, K. Lee, and D. G. Cahill, *Nat. Commun.* **5**, 4334 (2014).
- [28] G.-M. Choi, C.-H. Moon, B.-C. Min, K.-J. Lee, and D. G. Cahill, *Nat. Phys.* **11**, 576 (2015).
- [29] A. Kiriwara, K. Uchida, Y. Kajiwara, M. Ishida, Y. Nakamura, T. Manako, E. Saitoh, and S. Yorozu, *Nat. Mater.* **11**, 686 (2012).
- [30] S. Hu, H. Itoh, and T. Kimura, *NPG Asia Mater.* **6**, e127 (2014).
- [31] S. Takahashi and S. Maekawa, *Phys. Rev. B* **67**, 052409 (2003).
- [32] T. Kimura, J. Hamrle, Y. Otani, K. Tsukagoshi, and Y. Aoyagi, *Appl. Phys. Lett.* **85**, 3795 (2004).
- [33] T. Kimura, J. Hamrle, and Y. Otani, *Phys. Rev. B* **72**, 014461 (2005).
- [34] See Supplemental Material at <http://link.aps.org/supplemental/10.1103/PhysRevB.94.014416> for derivation of Eq. (1).
- [35] T. Kimura, J. Hamrle, Y. Otani, K. Tsukagoshi, and Y. Aoyagi, *Appl. Phys. Lett.* **85**, 5382 (2004).